



HAL
open science

Experimental study on the effects of direct sun radiation on the dynamic thermal behavior of a floor-heating system

Chihebedine Beji, Abdelatif Merabtine, Salim Mokraoui, Abdelhamid Kheiri,
Julien Kauffmann, Nahla Bouaziz

► To cite this version:

Chihebedine Beji, Abdelatif Merabtine, Salim Mokraoui, Abdelhamid Kheiri, Julien Kauffmann, et al.. Experimental study on the effects of direct sun radiation on the dynamic thermal behavior of a floor-heating system. *Solar Energy*, 2020, 204, pp.1-12. 10.1016/j.solener.2020.04.055 . hal-02877179

HAL Id: hal-02877179

<https://hal.science/hal-02877179>

Submitted on 20 May 2022

HAL is a multi-disciplinary open access archive for the deposit and dissemination of scientific research documents, whether they are published or not. The documents may come from teaching and research institutions in France or abroad, or from public or private research centers.

L'archive ouverte pluridisciplinaire **HAL**, est destinée au dépôt et à la diffusion de documents scientifiques de niveau recherche, publiés ou non, émanant des établissements d'enseignement et de recherche français ou étrangers, des laboratoires publics ou privés.



Distributed under a Creative Commons Attribution - NonCommercial 4.0 International License

1 **Experimental study on the effects of direct sun radiation on the dynamic** 2 **thermal behavior of a floor-heating system**

3 Chihebedine Beji^{a,b}, Abdelatif Merabtine^{b,c*}, Salim Mokraoui^d, Abdelhamid Kheiri^e, Julien
4 Kauffmann^b, Nahla Bouaziz^a

5
6 ^a*Université de Tunis El Manar, Ecole Nationale d'Ingénieurs de Tunis, unité de recherche*
7 *énergétique et environnement, BP 37, le belvédère 1002 Tunis, Tunisie.*

8 ^b*EPF School of Engineering, 2 rue Fernand Sastre, 10430, Rosières-Prés-Troyes, France*

9 ^c*ITHEMM, Université de Reims Champagne-Ardenne, Campus Moulin de la Housse, 51687*
10 *Reims Cedex, France*

11 ^d*College of Engineering, Chemical Engineering Department, King Saud University, Riyadh,*
12 *Saudi Arabia*

13 ^e*Université de Lorraine, Lemta, CNRS, Nancy. France*

14

15 **Abstract**

16 Radiant floor heating systems (FHSs) are considered reliable heating systems since they
17 maintain the indoor air temperature at the desired value and reduce its fluctuations more
18 efficiently than conventional heating systems do. However, FHSs require an optimal control
19 strategy especially when they are exposed to perturbations such as direct solar radiation or
20 unscheduled crowding. The present study investigates the dynamic thermal response of a FHS
21 exposed to a simulated direct solar radiation that is localized on its upper surface to quantify
22 the potential effects of this exposure and identify the subsequent control issues of the FHS.
23 Three experimental test scenarios were examined by varying the location of the sun patch and
24 its duration. The experimental results show that the tested FHS, primarily regulated by
25 controlling the indoor ambient air temperature, experiences a deficient regulation of the
26 indoor temperature, which leads to an overheating period depending on the sun patch intensity
27 and duration. An overheating of 4°C compared with the recommended maximum desired
28 value was recorded for duration of approximately 11.5 h after the sun patch was turned-off.
29 The experimental results may be used in further numerical studies to predict the thermal
30 behavior of FHSs exposed to sudden solar patches on their upper surfaces. The FHS design
31 elements (material, thickness, etc.), as well as the control procedures, must be reconsidered to
32 address the issue of overheating under such conditions.

33 **Keywords:** sun patch, direct solar radiation, floor-heating system, overheating rate,
34 experiments

35 **1. Introduction**

36 The increase in global energy consumption of buildings is an important issue since they
37 constitute a high share of the total global energy use as well as greenhouse gas emissions
38 (respectively 40% and 25% in UE (Li et al., 2019)). Hence, the building sector contributes
39 greatly to carbon emission and the rapid increase in global warming intensity, which the
40 international environmental treaties of Kyoto and Paris aim to lower. Researchers and
41 designers have suggested several solutions to overcome this issue, including more reasonable
42 use of current energy resources and the use of renewable energy sources.

43 In this context, floor-heating systems (FHSs) and floor-cooling systems (FCSs) have been the
44 subject of several studies focusing on analyzing their effect on indoor comfort conditions
45 (Merabtine et al., 2013; Karabay et al., 2013; Tian and Love, 2008), determining the factors
46 influencing their performances (Wang et al., 2014), and predicting their dynamic
47 performances under different conditions to enable a more efficient functioning (Joe and
48 Karava, 2019). FHSs and FCSs are usually classified as thermally active building systems
49 (TABS). Compared with conventional HVAC systems, the main advantage of these systems
50 is their ability to maintain a comfortable indoor air temperature varying from 22°C to 26°C in
51 the summer season and from 21°C to 24°C in the winter, with better spatial homogeneity and
52 overall comfortable conditions (ASHRAE, 2016; Kim and Olesen, 2015). In fact, according to
53 the International standards (ANSI/ASHRAE, 2010; ISO 7730, 2005) and to French guidelines
54 rules (CSTB, 2006), any part of the heating slab surface mustn't exceed 29°C or 28°C
55 respectively. However, one may understand that these rules are for the global heating floor
56 system design and are applicable only for this "artificial" of the surface provided by the
57 heating water, and hence, the part of the slab that is temporally heated by the sun patch is out
58 of the frame of this rule. This is also the case for the used heating film: the local surface
59 temperature of the later may exceed 28°C or 29°C. Elsewhere, the used infrared camera
60 provides measurement to confirm that the surface temperature doesn't exceed this upper limit.

61 The effect of solar radiation on the indoor environment has been the subject of several studies,
62 especially in the case of passive solar building designs where the solar energy is used to
63 enhance the thermal comfort conditions and reduce energy consumption. For FHSs, the
64 investigation of the effect of solar radiation inside a building is highly recommended because

65 of overheating in mid-season when the FHS is in use. Numerous studies concerning the
66 combination of a passive solar building design along with a FHS have been conducted. For
67 instance, Rodler et al. (2014) validated a numerical model capable of reproducing the
68 footprint of a sun patch on the floor and walls through an experimental work conducted at the
69 French EDF BESTLab. The study showed that a convenient use of stored solar energy in the
70 walls and floor enhances the overall building energy performances. A numerical study
71 conducted by Athienitis (1997) showed that a radiant heating floor allows the convenient use
72 of solar radiation since the floor thermal mass stores this energy, thus contributing to the
73 heating process over a long period. Two main cases along with a sensitivity analysis between
74 a fixed and a sinusoidal set point temperature controls were considered: the first was a clear
75 sky day scenario in which the solar radiation was set as $700 \text{ W}\cdot\text{m}^{-2}$, while the second was a
76 cloudy day scenario in which the maximum solar radiation was $100 \text{ W}\cdot\text{m}^{-2}$. The results
77 showed optimal outcomes in terms of maximizing the efficiency of the stored solar energy in
78 the floors, with the lowering of the initial temperature set point during the night and switching
79 to a half-sinusoidal control mode during the day.

80 The presence of solar radiation on the FHS and FCS surfaces depends on several parameters
81 such as the building orientation, the window size, and the shading system used. The intensity,
82 duration, and location of the sun patch strongly depend on atmospheric conditions (Holman,
83 2009). FHSs and FCSs may exhibit different thermal behaviors when exposed to solar beam
84 radiation. For instance, by using an experimental setup at the Tianjin railway station, Zhao et
85 al. (2013) introduced a simple method to predict the effect of solar radiation on the
86 performance of a radiant cooling system under steady-state conditions. They reported that the
87 cooling capacity of the FCS increased significantly when exposed to a solar beam of 40–100
88 $\text{W}\cdot\text{m}^{-2}$. Here, the material's emissivity is a key parameter for the radiative heat exchange
89 between the FHS and FCS surfaces and the surrounding walls. In another study, Zhao et al.
90 (2014) investigated the effect of material emissivity on longwave radiant heat exchange
91 between the surface of a radiant FCS and the surrounding indoor wall surfaces. The
92 introduced method demonstrated that the overall heat transfer coefficient decreases with a
93 decrease in emissivity, whereas the cooling capacity of the radiant FCS remarkably increased
94 to 80–155 $\text{W}\cdot\text{m}^{-2}$ when exposed to direct solar radiation.

95 For the special case of FHSs, quantifying the effect of the presence of direct solar radiation
96 on its surface is important since local overheating may occur, leading to an increase in air
97 temperature to unacceptable values causing discomfort to the occupant. In this context,

98 Athienitis and Chen (2000) introduced a three-dimensional numerical model to analyze the
99 effect of the presence of intense solar beam radiation on the floor surface of a room equipped
100 with a radiant heating system. The study considered two major cases of uncarpeted and partly
101 carpeted floors, and the simulation results revealed that the local temperature of the floor area
102 exposed to solar radiations was higher than that of the non-exposed area by 8°C, and the
103 difference can be as high as 15°C in the case of non-uniformly covered floor. The transient
104 nature of solar radiation and the high inertial effect on the FHS induce a special and non-
105 obvious behavior. Benzaama et al. (2016) conducted a numerical study to quantify the effect
106 of a sun patch on the indoor air and floor temperatures of a room equipped with a FHS. The
107 numerical study was conducted using a model combining the two commercial simulation
108 software TRNSYS and ANSYS Fluent. The results revealed that on a sunny day, the indoor
109 air temperature increased by 2°C, while the temperature of the exposed floor surface was
110 13°C higher than that of the shaded area.

111 The main problem of FHSs is their control, mainly the ability of the adopted control strategy
112 to reduce the overheating whenever an unexpected perturbation occurs, such as direct sun
113 radiation on the floor. Conventional control strategies are classified into three main
114 categories: the on-off temperature control, weather-compensated control, and PID control
115 (Privara et al., 2011). These types of control were then followed by the model predictive
116 control strategy (MPC) that allows a more adaptive response of a radiant system toward
117 unexpected perturbations of their environments. MPC has been discussed in several studies
118 (Joe and Karava, 2019; Privara et al., 2011; Candanedo et al., 2011) and has been proved to
119 be an efficient tool for systems' command adjustment to provide optimal control.

120 The available literature shows that the number of studies on the investigation of the solar
121 radiation effect on thermally active building systems is higher in the case of radiant cooling
122 systems. This is because, for cooling purposes, the internal building environment is highly
123 sensitive to the presence of a heat source, such as solar radiation, which may affect the indoor
124 air temperature and the air conditioning system performance. Fewer studies have been
125 devoted to the effect of direct sun radiation (Athienitis, 1997; Athienitis and Chen, 2000;
126 Benzaama et al., 2016) and the thermal response of radiant floor heating. The majority of
127 works was performed using analytical or numerical models. This is because FHS designers
128 tend to neglect solar radiation during the heating season even if clear sky days with intense
129 solar radiations may occur during mid-season. To our best knowledge, there is no published
130 experimental study on the effect of a direct solar heat flux on a radiant FHS and its dynamic

131 performance. For this reason, an experimental study explicitly evaluating the effect of direct
132 solar radiations on the FHS performance is particularly important for a more accurate design
133 of FHSs and their control strategy. Such study would provide a more realistic explanation of
134 the thermal behavior of FHSs under direct solar radiations, thus providing a smart adaptive
135 control strategy that utilizes the stored solar energy as a supplement to the floor thermal mass.

136 The aim of the present scientific contribution is to fill the gap sensed in the current state-of-
137 the-art by performing an experimental study on the effect of direct solar radiation on a room
138 equipped with a radiant FHS. The experimental data obtained from this study can be used to
139 validate further numerical models. The overall objective is to help designers to a better
140 conception and optimization of such systems.

141 The paper is organized as follows: the next section describes the test cell along with the
142 equipment used in this work. Then, the experimental protocols regarding the three realistic
143 scenarios are depicted. The last section is devoted to the interpretation of results and their
144 discussion followed by the general conclusions and perspectives.

145 **2. Experimental setup**

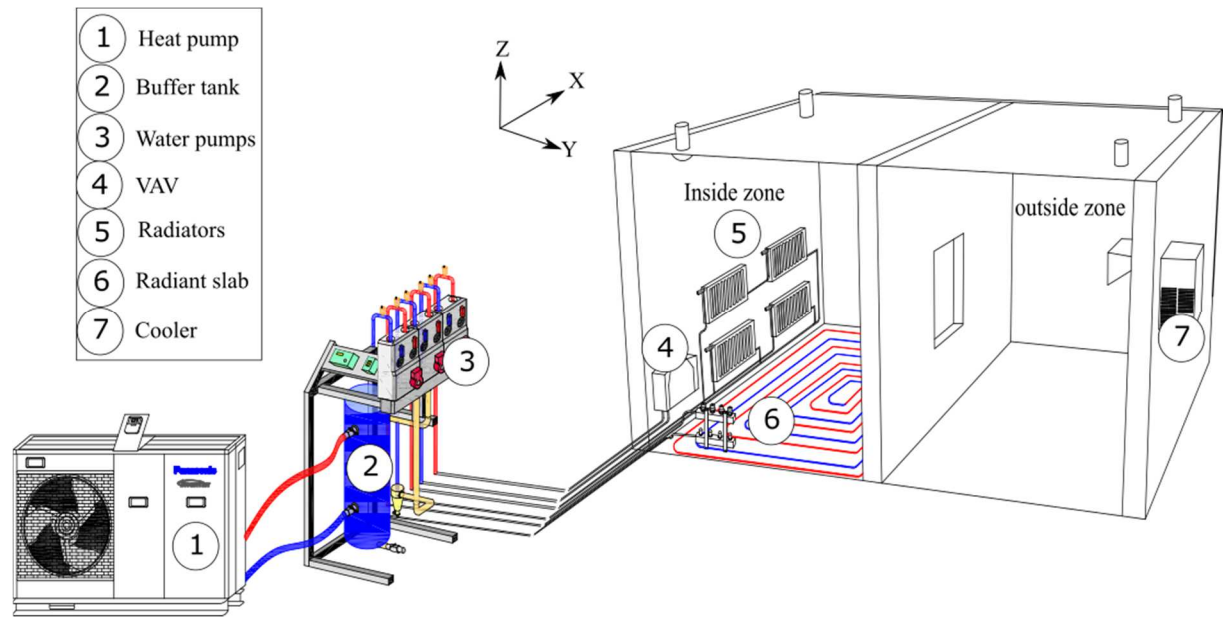
146 To investigate the effect of direct solar radiations on the thermal performance of a FHS, a
147 series of experiments was conducted in a full-scale test cell facility located in the EPF
148 Graduate School of Engineering in Troyes (France). The test cell facility (Fig. 1) comprises
149 two climatic chambers with a total area of 11 m² and a height of 2.1 m. A 0.5 m highly
150 insulated wall essentially made from wood and hemp wool insulating materials separates the
151 climatic chambers. The left chamber, called the inside zone (Fig. 1), is equipped with a FHS
152 comprising a 51-m-long embedded cross-linked polyethylene tube placed under a 5-cm-thick
153 anhydrite screed slab, over which a 6-cm-thick insulation layer essentially made from wood
154 fibers is placed. The main purpose of this climatic chamber is to reproduce the actual
155 conditions of a warm, heated indoor environment by the means of a radiant heating floor.



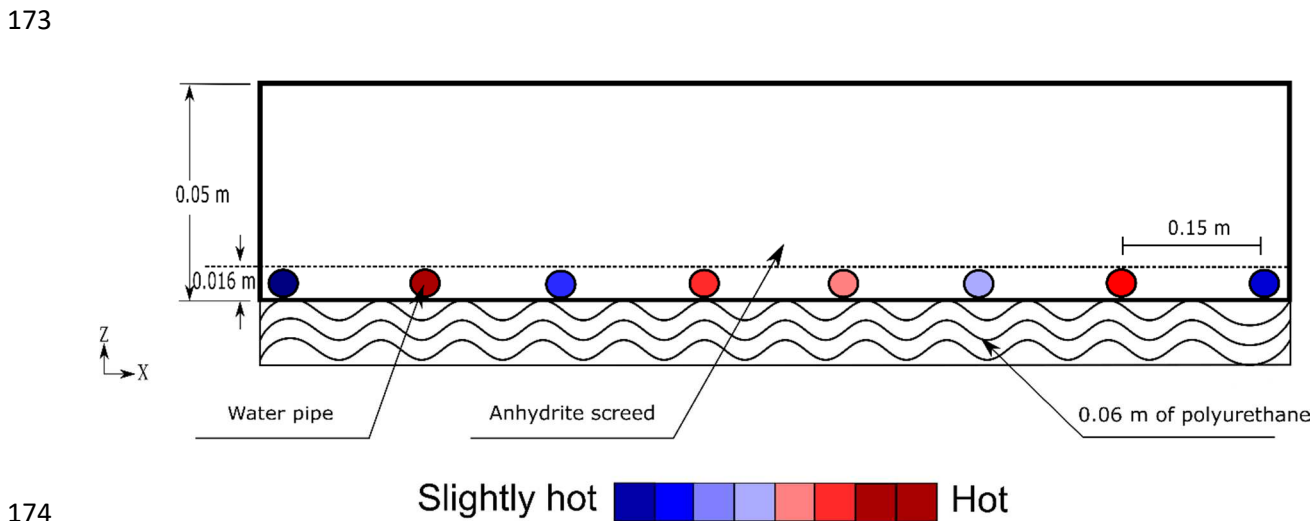
156

157 Figure 1: Outer view of the experimental test facility.

158 The climatic chamber on the right side is called the outside zone and is equipped with a
159 powerful cooler capable of reproducing the external cold weather conditions. It must be noted
160 that both the cells of the test facility are equipped with different HVAC systems and that
161 much of these systems are located in the heated cell, which includes a radiant slab, four
162 radiators, and a fan coil unit (variable air volume type). All the HVAC systems attached to the
163 test facility are shown in Fig. 2, while the radiant slab structure is described in Fig. 3. More
164 information regarding material characteristics are given in table 1. A radiant heating film is
165 fixed on the radiant slab to simulate solar radiation (Fig. 4). A heat pump, a system of the
166 buffer tank, a pump, and a three-way valve, ensures the water heating process. All the chosen
167 devices are capable of reproducing actual thermal conditions when a FHS is used in buildings.
168 Furthermore, all the present devices in the inside zone are directly controlled through an
169 external computer that also collects the indoor climatic data, tracked every minute through a
170 set of multiple sensors placed all over the climatic chambers and the radiant slab surface.



171
172 Figure 2: Overview of the HVAC systems.



174
175 Figure 3: Cross section view of the radiant slab

176 Table 1: Material characteristics

Designation	Characteristics
Insulation materials of the test cell	Hemp wool $\rho = 25 \text{ kgm}^{-3}$; $\lambda = 0.04 \text{ Wm}^{-1}\text{K}^{-1}$
	Wood fibers $\rho = 40 \text{ kgm}^{-3}$; $\lambda = 0.04 \text{ Wm}^{-1}\text{K}^{-1}$
HVAC systems	Air ventilation system consisting on a dual-flow ventilation equipped with enthalpy wheels.
	Air conditioning system is set to maintain the cold room at a temperature between $-18 \text{ }^\circ\text{C}$ and $25 \text{ }^\circ\text{C}$.

The FHS consists of a tube coil placed on a wood fibers insulation panel and covered with an anhydrite screed.

Anhydrite screed: $e = 50 \text{ mm}$; $\rho = 1900 \text{ kgm}^{-3}$; $\lambda = 1.2 \text{ Wm}^{-1}\text{K}^{-1}$; $C_p = 1000 \text{ Jkg}^{-1}\text{K}^{-1}$; $\varepsilon = 0.95$; $S_{FHS} = 5.5 \text{ m}^2$



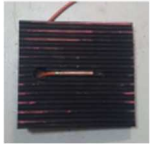

Insulation panel: $e = 60 \text{ mm}$; $\rho = 40 \text{ kgm}^{-3}$; $\lambda = 0.04 \text{ Wm}^{-1}\text{K}^{-1}$; $C_p = 2100 \text{ Jkg}^{-1}\text{K}^{-1}$

Tube coil is a cross-linked polyethylene tube $D_e = 16 \text{ mm}$; $D_i = 13 \text{ mm}$; $L = 51 \text{ m}$; $\rho = 933 \text{ kgm}^{-3}$; $\lambda = 0.4 \text{ Wm}^{-1}\text{K}^{-1}$; $\dot{V} = 0.02 \text{ ls}^{-1}$; roughness = 0.007 mm.m-1; Distance between pipes = 0.15 m.

177

178 The list of installed sensors and the equipment used during the tests are given in Table 2. The
 179 composition of this test facility and its technical criteria are suitable for conducting
 180 comprehensive studies to evaluate the performance of radiant heating floors. In particular, it
 181 allows the simulation and analysis of the potential impact of a beam solar radiation on the
 182 indoor air temperature and the FHS thermal response for different case studies.

183 Table 2: List of measuring equipment.

Instrument	Measured parameter	Number	Range	Accuracy	Indication
KLU 100 sensor	outdoor RH and air temperature sensor	1	[-50,50] °C [0,100] %	±2 % at 25°C ±0.5 °C at 0°C	
KLH 100 sensor	Indoor RH and air temperature sensor	1	[-50,50] °C [0,100] %	±2 % at 25°C ±0.5 °C at 0°C	
PT 100 sensor	Surface temperature sensor	2	[-20,100] °C	±0.3 °C at 0°C	
PT 1000 sensor	Depth temperature sensor	2	[-20,100] °C	±0.3 °C at 0°C	

ASTF PT 1000	Mean radiant temperature sensor	1	$[-30,75] \text{ } ^\circ\text{C}$	$\pm 0,5^\circ\text{C}$ at 25°C	
TEPK PT 1000	Inlet and outlet water temperature sensor	2	$[-20,80]^\circ\text{C}$	$\pm 0,3 \text{ } ^\circ\text{C}$ at 0°C	
FLUKE TIR 105	Infrared thermal camera	1	$[-20,150] \text{ } ^\circ\text{C}$	$\pm 0,1^\circ\text{C}$ at 30°C	
AHLBORN FQA019C	Surface heat flux meter	2	$[-260, 260] \text{ mV, } <120 \text{ } ^\circ\text{C}$	$\pm 0.01 \text{ mV}$ For $\pm 0.12 \text{ } ^\circ\text{C}$	
KLK 100 sensor	Indoor RH and ambient air temperature sensor	1	$[-50,50] \text{ } ^\circ\text{C}$ $[0,100] \%$	$\pm 3\%$ at 25°C $\pm 0,5^\circ\text{C}$ at 25°C	

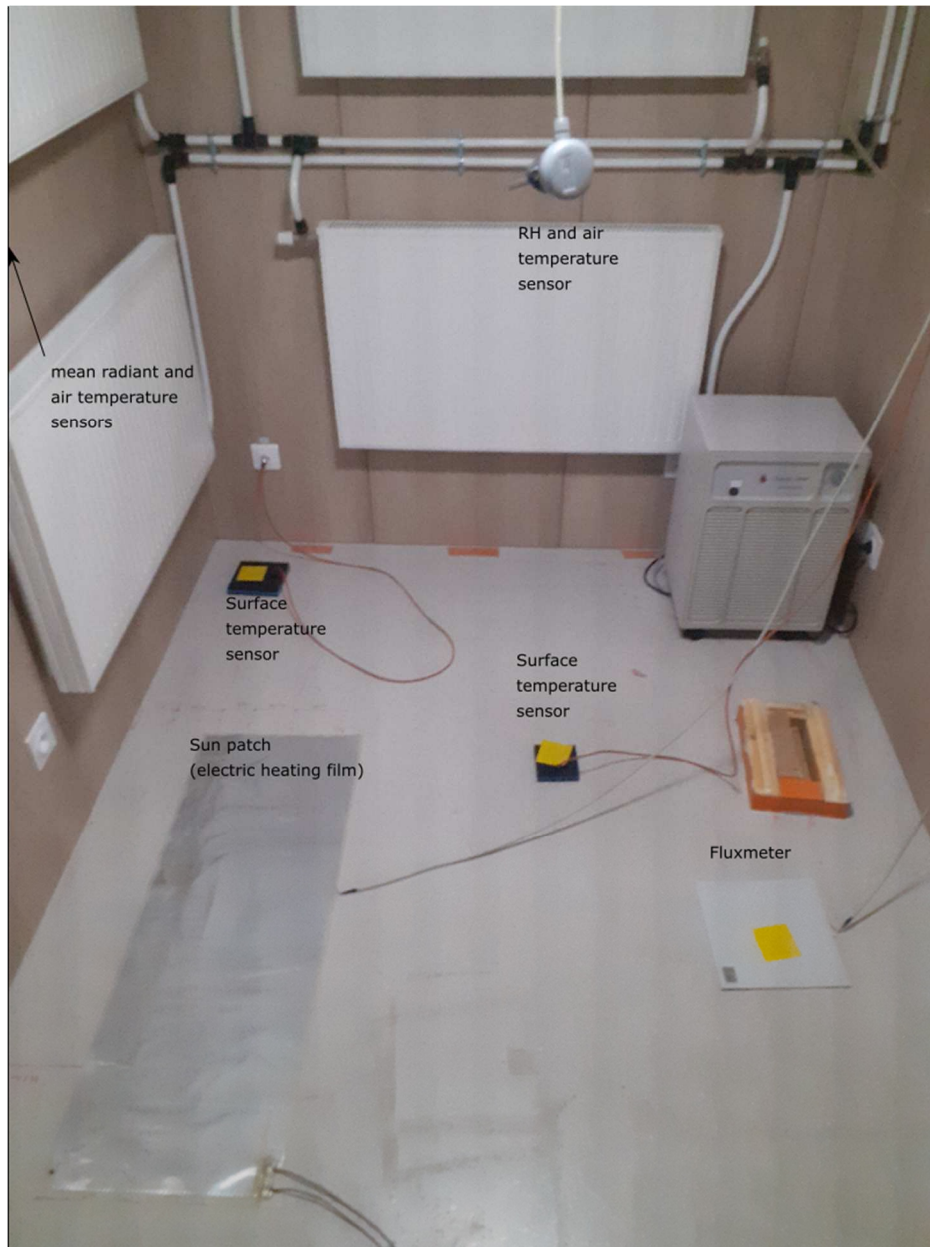
184

185 Furthermore, it is important to note that all the installed HVAC systems are directly powered
186 by a heat pump located outside the climatic chambers. Its functioning mode depends on the
187 cooling and heating requirements of the case study, where the desired set point temperatures
188 of both the rooms are the ultimate parameters that need to be considered. The set point
189 temperature depends on the desired indoor thermal comfort temperature for heating purposes,
190 which usually ranges between 21°C and 24°C , as given by ASHRAE (2016). However, the
191 volume flow rate of hot water is an important parameter for controlling the heating process of
192 a room equipped with a radiant heating slab. In the present set of experiments, the inlet water
193 temperature is controlled by the three-way valve according to the outdoor temperature and the
194 flow rate of the hot water, which is controlled by a thermostatic valve. These valves inject hot
195 water to the radiant slab until the air temperature stabilizes around the initial set point
196 temperature before starting a progressive shutdown process, where heating is sustained

197 through the thermal inertia of the radiant slab. It is noteworthy that these valves are highly
198 sensitive to any minor changes in the ambient room temperature.

199 **3. Experimental protocol**

200 The experiment involves the analysis of three different scenarios under two fixed parameters
201 in the winter season. The fixed parameters were the air temperatures of the two climatic
202 chambers representing the indoor room conditions and the outside weather conditions,
203 respectively. The room equipped with a FHS is heated to a set point temperature of 23°C and
204 subjected to a simulated direct solar radiation with a localized patch, while the external
205 temperature is fixed as 5°C. As shown in Fig. 4, the solar patch was experimentally simulated
206 by an electric heating film with a modulated power that varies from $203 \pm 22 \text{ W}\cdot\text{m}^{-2}$ to $718 \pm$
207 $58 \text{ W}\cdot\text{m}^{-2}$. The floor heating film has dimensions of $0.400 \text{ m} \times 1.065 \text{ m}$. The lower surface of
208 the film provides heat directly to the floor slab, while the upper surface exchanges heat with
209 the surrounding and ambient air by radiation and convection, respectively. The difference
210 between the three considered scenarios is the location and duration of the heating film on the
211 floor surface.



212

213 Figure 4: Actual view of the inside zone with the electric heating film in the first test scenario.

214 In the first experimental test scenario, the heating film is positioned as shown in Fig. 5a to

215 simulate an incoming solar radiation from the South; the solar radiation coming from this

216 direction remains for a sufficient time. In the second scenario (Fig. 5b), the heating film is

217 placed perpendicular to the previous position to simulate an incoming solar radiation from the

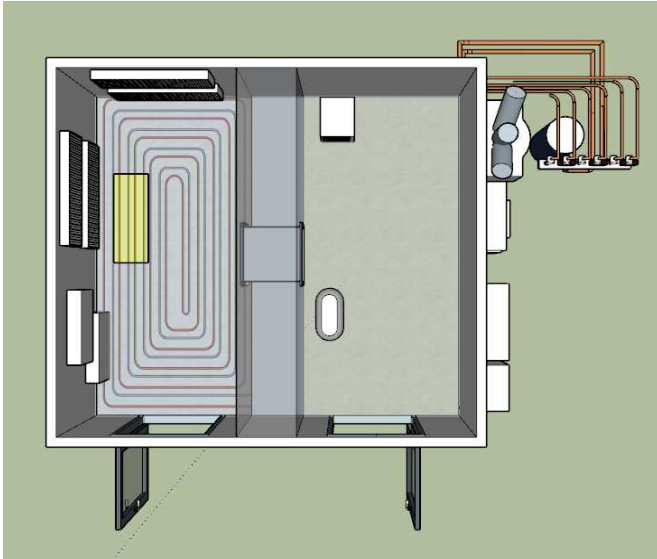
218 East or West direction. The heating film running time was set as 2 h in the first two

219 experimental scenarios. In the third scenario (Fig. 5c), the heating film was initially placed in

220 the same position as that in the first test and then moved horizontally 40 cm toward the Y-

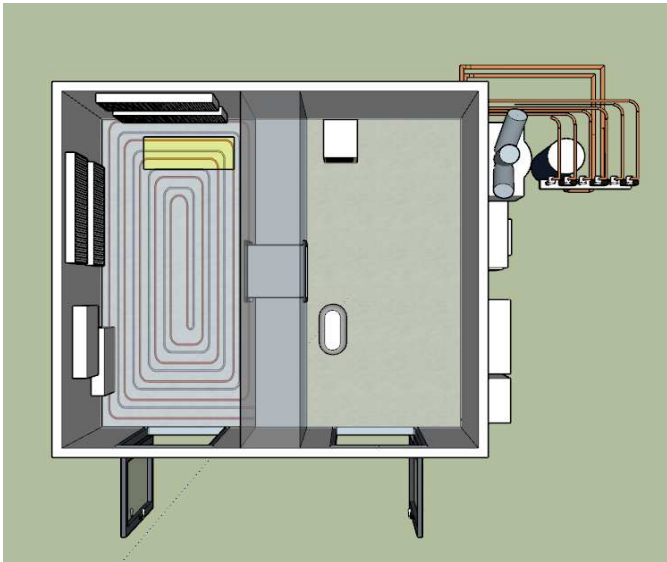
221 direction every 2 h. Thus, the third test reproduces a moving sun patch coming from the South

222 for a total duration of 6 h.



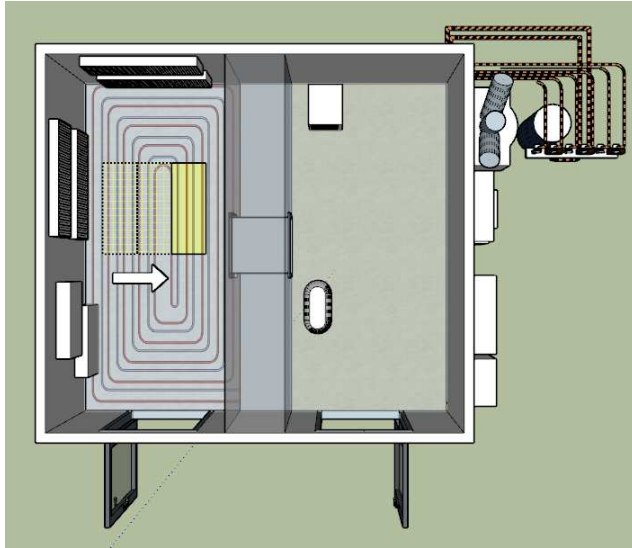
223

224 (a)



225

226 (b)

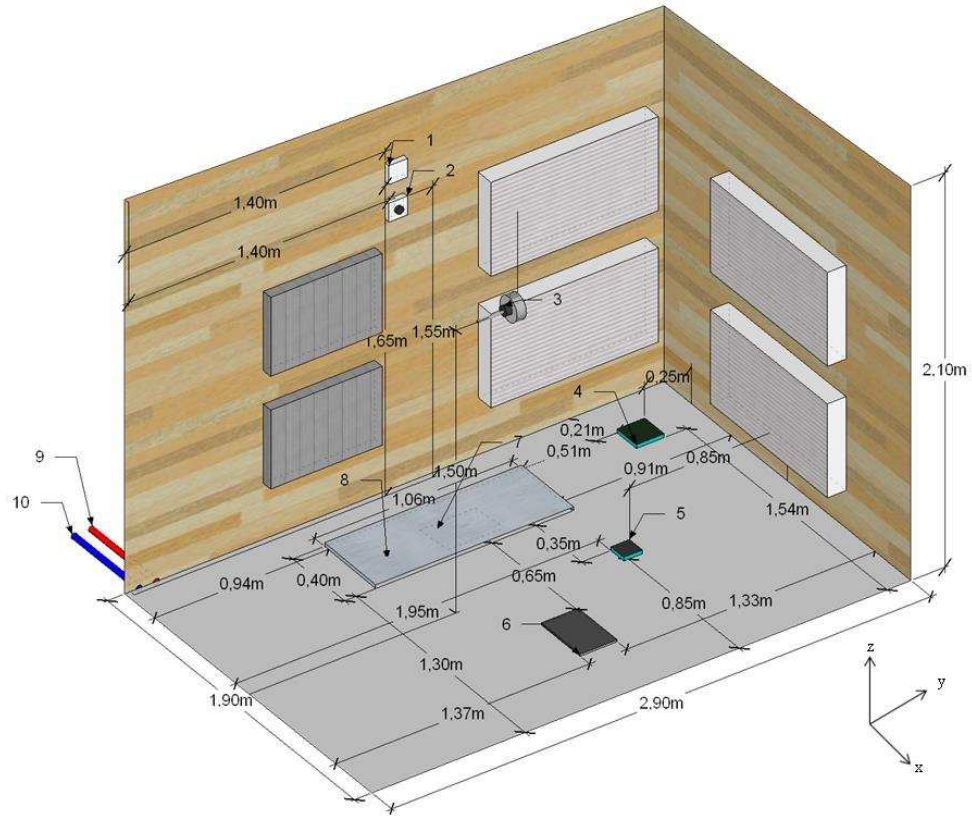


227

228 (c)

229 Figure 5: Location of the radiant film. (a) First scenario (solar radiation from South); (b)
230 second scenario (solar radiation from East/West); (c) third scenario (moving location; south
231 orientation).

232 All the measuring points and instruments exact locations are depicted in Fig 6. The electric
233 power of the heating film was set to achieve $700 \text{ W}\cdot\text{m}^{-2}$, which represents the solar intensity
234 on a clear sky day in the winter season (Athienitis, 1997).

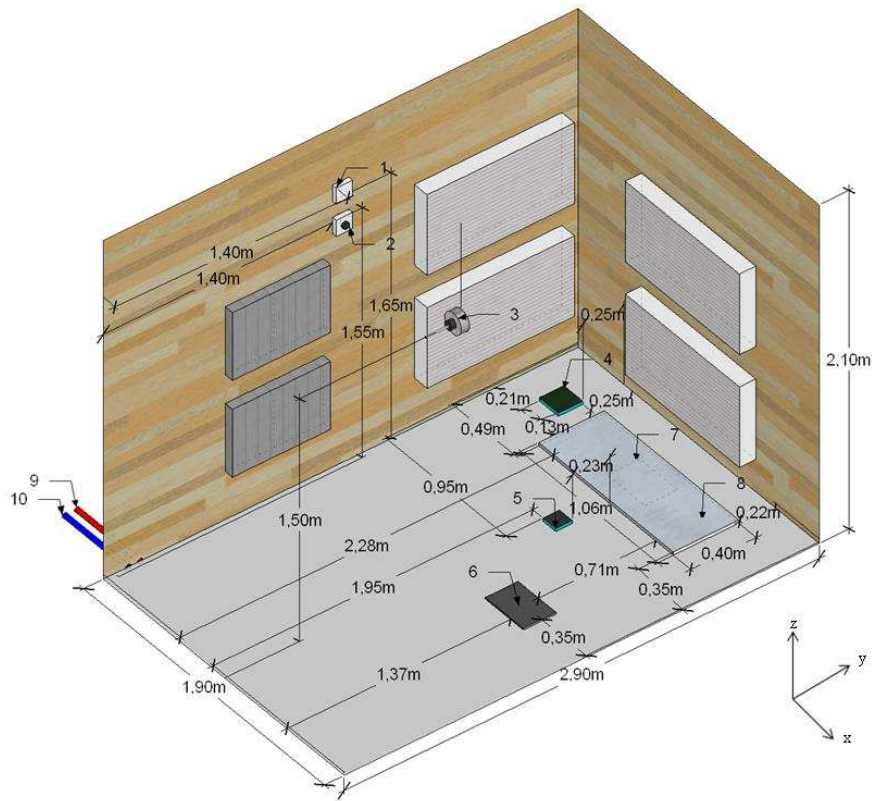


235

236 (a)

237

238



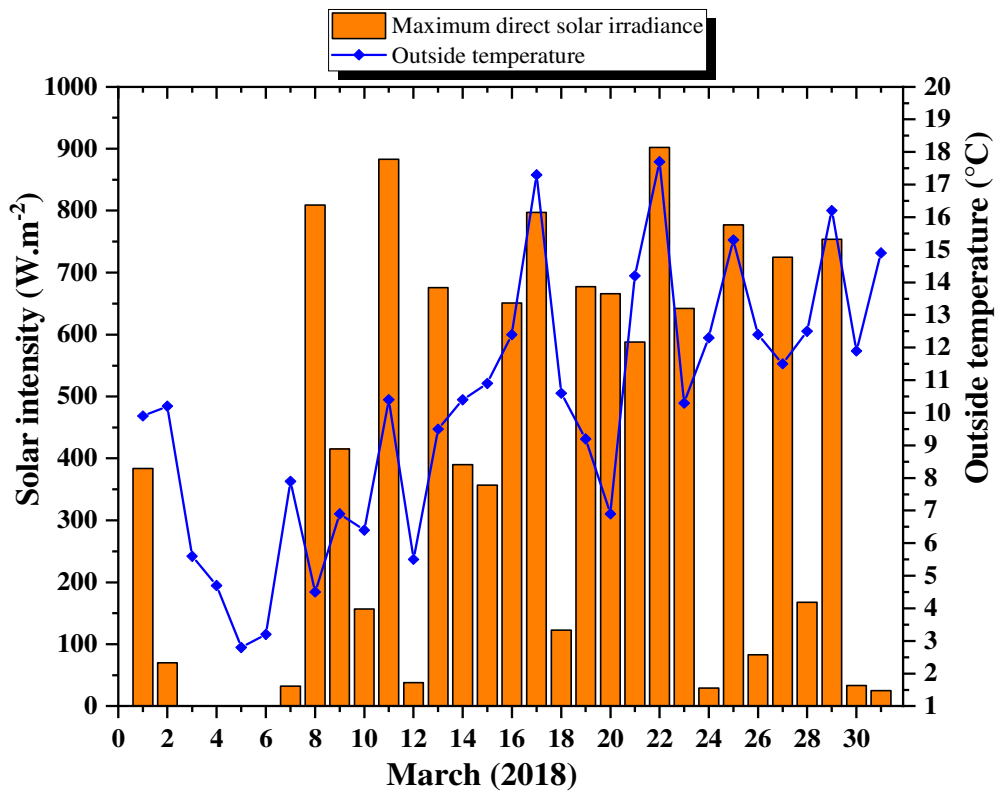
239

240 (b)

241 Figure 6: Location of measuring points and instruments. (a) first and third test scenarios; (b)
 242 second test scenario. (1) and (3) RH and air temperature sensors; (2) mean radiant temperature
 243 sensor; (4) and (5) surface temperature sensors; (6) and (7) flux meters; (8) heating film; (9)
 244 and (10) water temperature sensors.

245 As for the actual total direct solar radiation on the earth's surface for March 2018, Fig. 7
 246 illustrates the data collected by a weather station located in Troyes 11.5 km from the test cell
 247 facility (Weather Channel, 2019). The recorded data show that the solar intensity may exceed
 248 $700 \text{ W} \cdot \text{m}^{-2}$ on certain cold sunny days.

249



250

251 Figure 7: Recorded direct solar radiation on the earth's surface in Troyes during March
 252 2018.

253 The amount of heat transmitted to the radiant floor is approximately 70–80 % lower than the
 254 total film intensity because of the g-value. This regression is because of the progressive
 255 decrease in solar irradiance intensity due to the glazing type and glass coatings (Singh and
 256 Garg, 2010).

257 During the tests and for the three test scenarios, the location of the sensors used to record the
 258 data remained unchanged. The sensor type and locations are as follows:

- 259 • Air and relative humidity sensors were placed 1.8 m above the floor in both the
 260 climatic chambers.
- 261 • A sensor to track the variations in radiant temperature was installed in the heated
 262 room.
- 263 • Two surface temperature sensors were placed away from the heating film to minimize
 264 the effects of localized heat that it may cause. The location of those sensors was
 265 chosen in a way that their average is close to the actual average surface temperature by
 266 fixing one sensor on a surface which is above the inlet water tube, while the second

267 one was fixed in that above the outlet water tube. Thermal infrared images were taken
268 to identify those locations. According to those images, we can check if either local
269 surface temperatures (according to NF DTU 65.14 P1) or average temperature is under
270 the upper limit of 28 °C.

- 271 • Two depth sensors were placed in the radiant floor of the heated room at heights of 2.6
272 cm and 3.6 cm, respectively, from the insulation layer carrying the embedded pipes.
- 273 • Two heat flux meters were used: the first was placed under the radiant film to measure
274 the amount of heat transmitted to the radiant slab, while the second was placed near
275 the insulated separation wall of the two rooms.

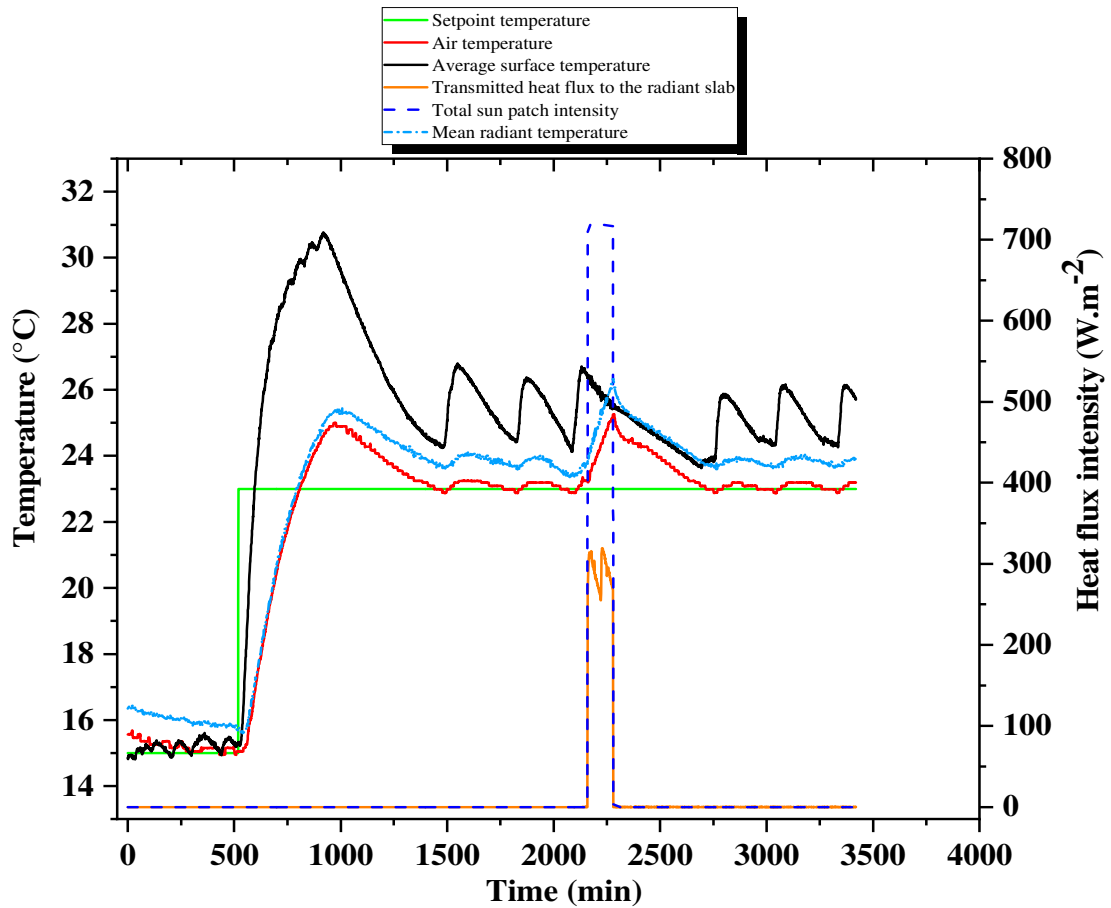
276 **4. Results and discussion**

277 **4.1. First scenario**

278 In the first experimental scenario, the air temperature of the inside zone was maintained at
279 15°C and then the FHS system was turned-on to heat the climatic chamber to the ambient air
280 set point fixed as 23°C. Meanwhile, the outside zone, i.e., the cold climatic chamber
281 temperature was set as 5°C. As shown in Fig. 8, at the beginning of the test, the average
282 surface temperature reaches 31°C, exceeding the permissible limit of 28°C as per the legal
283 regulation. It is noticed that the measured surface temperatures are relatively similar to the
284 average surface temperature which allows assuming that the surface temperature is
285 homogenous.

286 This is related to the thermostatic valve functioning, which exclusively depends on the desired
287 ambient air temperature, and thus, the valve operates even when the surface temperature
288 exceeds 28°C, as shown in Fig. 9. This aspect highlights the fact that such a regulation, which
289 depends solely on the air temperature, can cause significant floor overheating. Fig. 9 shows
290 the relationship between the thermostatic valve-opening rate and the heating floor surface and
291 indoor air temperatures. As can be seen, the thermostatic valve-opening rate shows six timely
292 small localized maximums after instant $t=1500$ min and each of them produces similar
293 localized maximums of the ambient air temperature. This indicates that even if the opening
294 rate does not exceed 10%, it can significantly affect the surface temperature, and indirectly,
295 the air temperature.

296

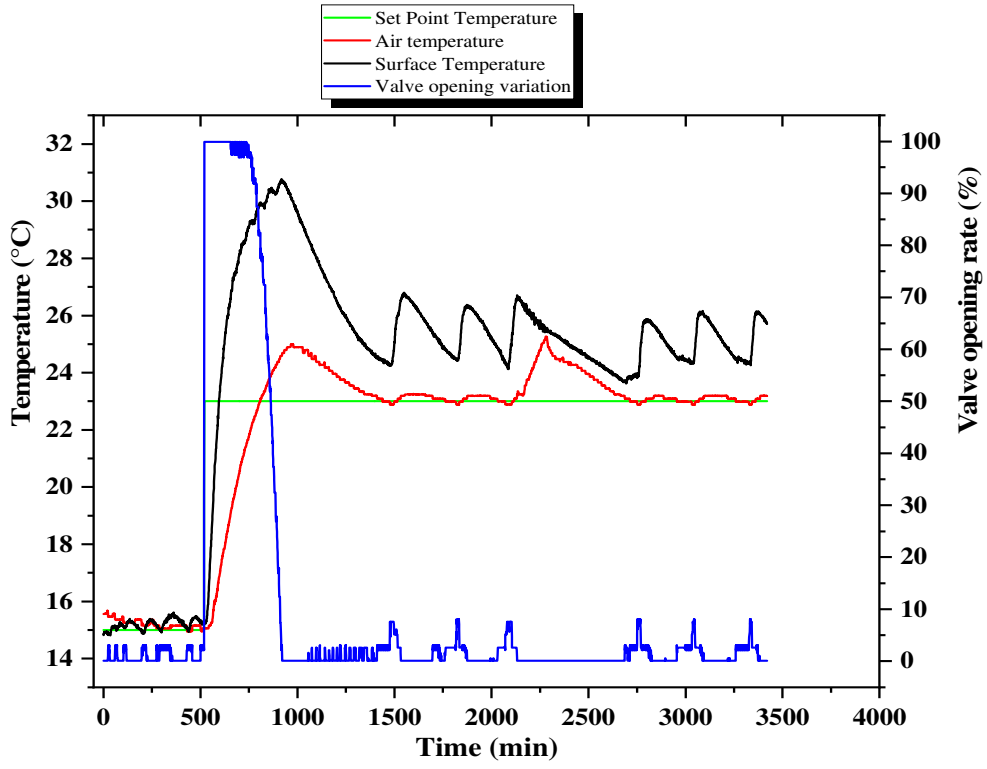


297

298 Figure 8: Average surface temperature, air temperature, and direct solar radiation intensity
 299 profiles in the first test scenario.

300 Further, the indoor air temperature initially increases when the thermostatic valve-opening
 301 rate is 100% and reaches its set point of 23°C; however, it does not stop despite the decrease
 302 in the valve-opening rate to 0%. Hence, the air temperature exceeds 24°C and decreases after
 303 some delay time (after the valve is turned-off). When the air temperature starts to stabilize at
 304 the desired set point, around t=1500 min, the surface temperature shows two minor
 305 fluctuations. This is an expected behavior because the thermostatic valve regularly injects a
 306 small amount of hot water to prevent the set point temperature from dropping below 23°C.
 307 This can be observed in Fig. 10, which shows many fluctuations of the inlet water
 308 temperature as the thermostatic valve operates.

309

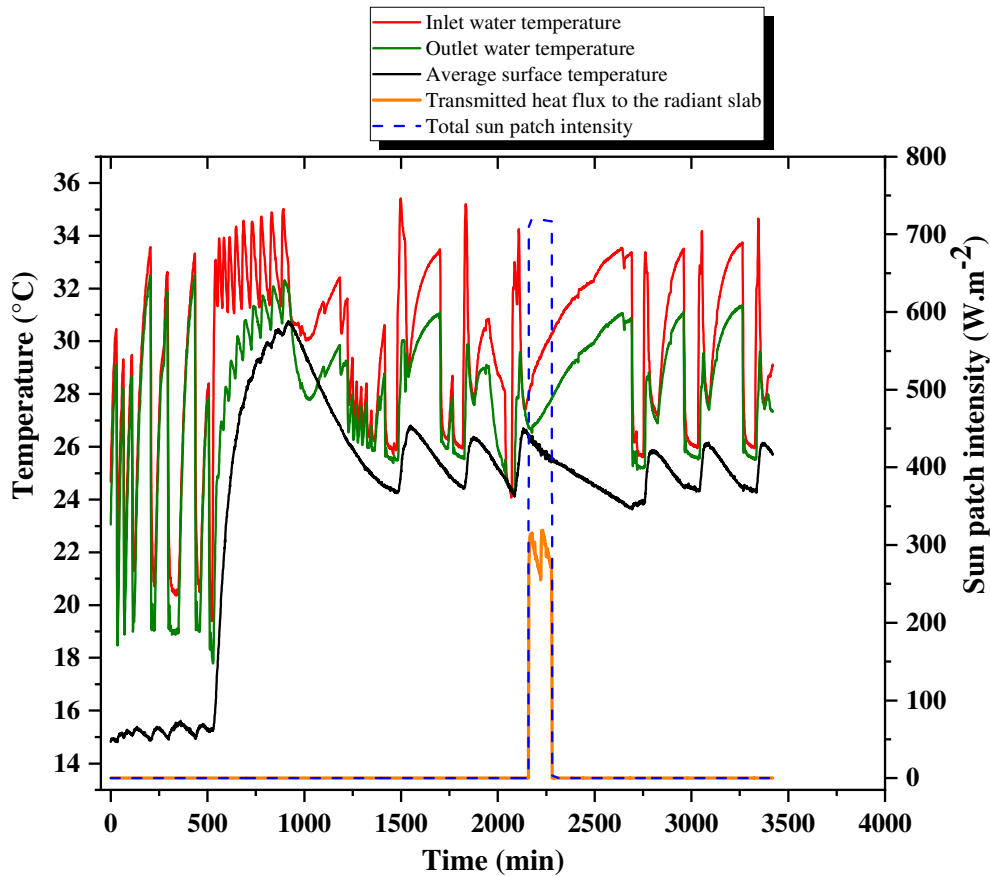


310

311

312 Figure 9: Variation in thermostatic valve opening during the first test scenario.

313



314

315 Figure 10: Variation in inlet and outlet water temperatures during the first test scenario.

316 When the measured air temperature reaches an approximately steady state at 23°C, the
 317 heating film is turned on with an intensity of 718 W·m⁻² for 2 h to simulate a localized direct
 318 solar radiation on the FHS. This is to achieve realistic conditions since the sun's position
 319 constantly changes during the day. As the heating film is turned on, the air temperature
 320 rapidly exceeds 23°C and reaches 25°C with a delay time, thus exceeding the recommended
 321 upper limit of 24°C for 280 min.

322 Fig. 9 and 10 shows that the fluctuation in the average radiant floor surface temperature is the
 323 same as that before the sun patch was introduced; hence, it remains unaffected by the
 324 presence of sun patch for 2 h. It can be concluded that in the first experimental scenario, the
 325 location, emission intensity, and duration of the sun patch on the radiant floor did not
 326 overheat the heating floor surface in a manner that exceeds the limit of 28°C. Nevertheless,
 327 the room's air temperature exceeds the set point value over the duration of 650 min.

328 The overheating rates, OR^s and OR^a , are defined as the durations over which the average
329 surface temperature and indoor air temperature exceed the recommended upper limits of 28
330 °C and 24 °C, respectively. Thus:

$$331 \begin{cases} OR^s = \frac{t_o^s}{t} \\ OR^a = \frac{t_o^a}{t} \end{cases} \quad (1)$$

332 In the first experimental test scenario, the overheating rates related to the indoor air
333 temperature and surface temperature are 8.2 % and 0 %, respectively. It seems that the
334 overheating rates depend on the main thermal characteristics of the heating slab and the sun
335 patch intensity and duration. This indicates an important issue regarding the current regulation
336 system of the FHS, i.e., the thermostatic valve continues to inject hot water, as its regulation
337 depends exclusively on the ambient air temperature, while the radiant slab surface
338 temperature exceeds the maximum standard value of 28°C. A more convenient regulation
339 system must take into account the surface temperature to avoid exceeding the maximum
340 standard value.

341 **4.2. Second scenario**

342 The second experimental test scenario was started with the same parameters as those of the
343 first test scenario (i.e., 15°C in the inside zone and 5°C in the outside zone). After a while, the
344 ambient air temperature in the inside zone was set as 23°C. The major modification was the
345 change in the location of the radiant film, which was moved to the normal position with
346 respect to the previous one to simulate a direct solar radiation coming from the East or West
347 direction in the early hours of the morning or anytime in the evening before sunrise (Fig. 11).
348 It should be noted that this arrangement allows the investigation of the effect of a sun patch
349 on the dynamic thermal behavior of the FHS for a different set of embedded pipes in the floor.

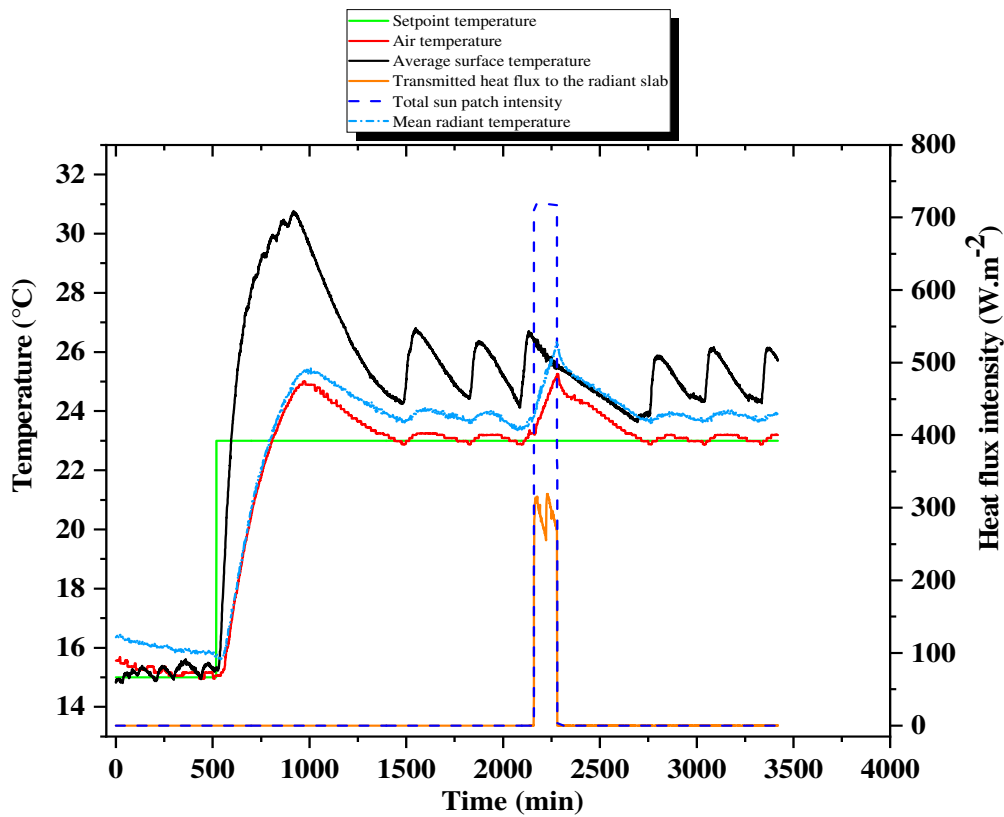


350

351 Figure 11: Overview of the test cell and the radiant film location in the second experimental
352 test scenario.

353 Fig. 12 shows that before turning on the heating film, the fluctuations in air temperature and
354 surface temperature are similar to those in the first test. As in the first test scenario,
355 immediately after the heating film was turned on, the air temperature increased almost
356 instantly, while the average surface temperature increased gradually, reaching approximately
357 27°C and then decreasing to the initial values before turning on the heating film. The average
358 surface temperature profile (Fig. 10) is different from that in the first scenario. This is because
359 in the second scenario, one of the surface temperature sensors is closest to the radiant film
360 (Fig. 11) and is thus more affected by the presence of the hot patch. In the case of air
361 temperature, a maximum overheating of 2°C compared with the set point temperature is
362 observed. Hence, the overheating rates are 6.7% and 0%, respectively.

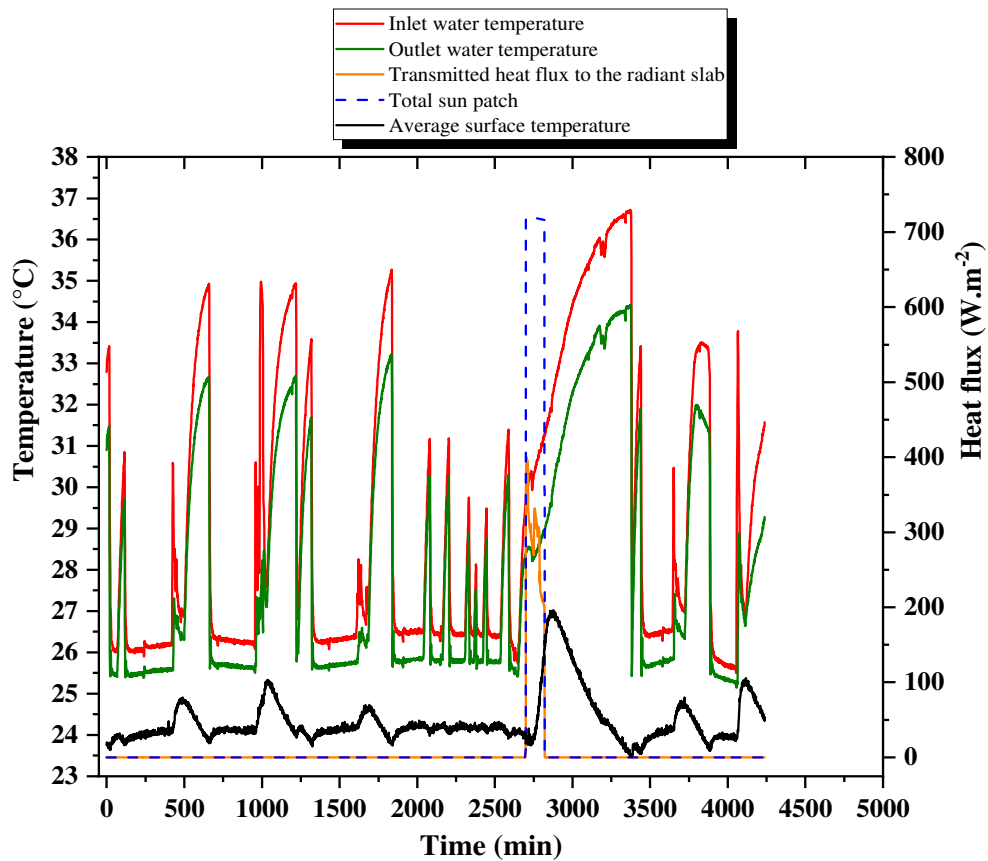
363



364

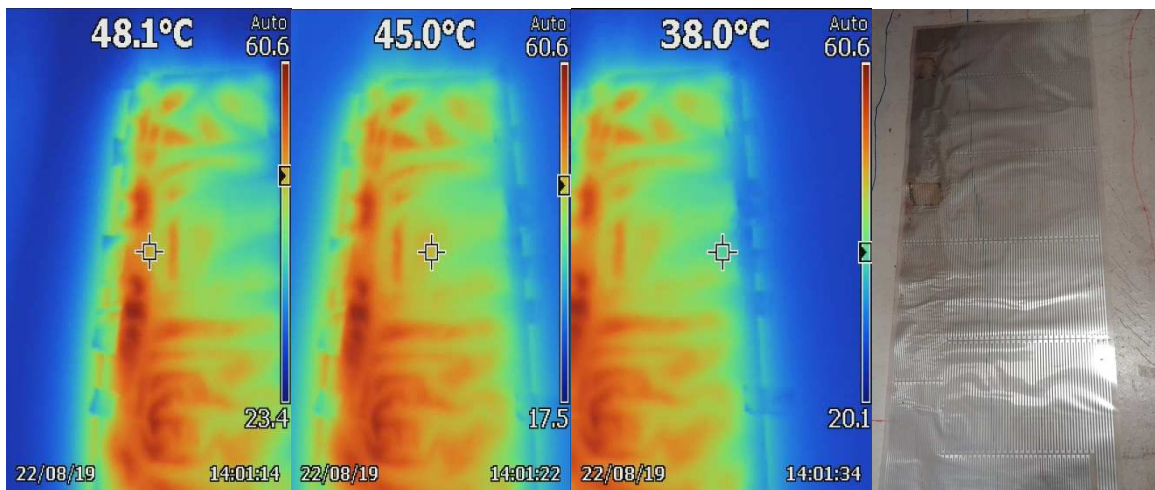
365 Figure 12: Average surface temperature, air temperature, and direct solar radiation intensity
 366 profiles in the second test scenario.

367 Furthermore, as illustrated in Fig. 13, the inlet and outlet water temperature profiles are
 368 similar to those in the first scenario. The change in the sun patch position increased the inlet
 369 water temperature to over 36°C, which is higher than that obtained in the previous test.
 370 Moreover, the heat transmitted by the film to the FHS is not uniform, as shown in the thermal
 371 images taken by an infrared thermal camera (Fig. 14). The thermal images show that the
 372 upper surface temperature of the exposed floor is 11–21°C higher than that of the non-
 373 exposed area, which represents a serious localized and unavoidable overheating problem. This
 374 was previously highlighted and modeled by Athienitis (1997). Some floor coverings such as
 375 carpet, wood, and so on with low thermal effusivity b could be useful to draw heat out of a
 376 bare feet ($b = 7 \text{ J.m}^{-2}.\text{K}^{-1}.\text{s}^{-1/2}$ for the oak wood versus 25 for the concrete).



377

378 Figure 13: Inlet and outlet water temperature profiles in the second test scenario.

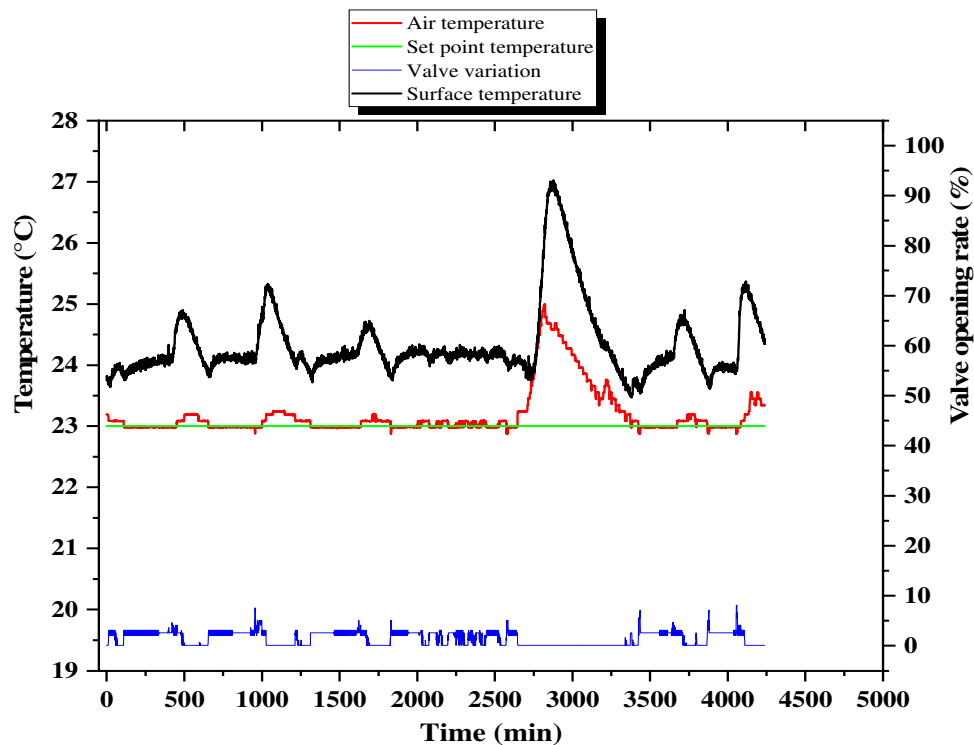


379

380

381 Figures 14: Infrared thermal images showing the electric film surface temperature profile.

382 Further, the thermostatic valve-opening rate exhibited similar behavior as that seen in the first
 383 test for the two phases, i.e., before turning on and after turning off the heating film, as shown
 384 in Fig. 15.



385

386 Figure 15: Variation in thermostatic valve-opening rate in the second test scenario.

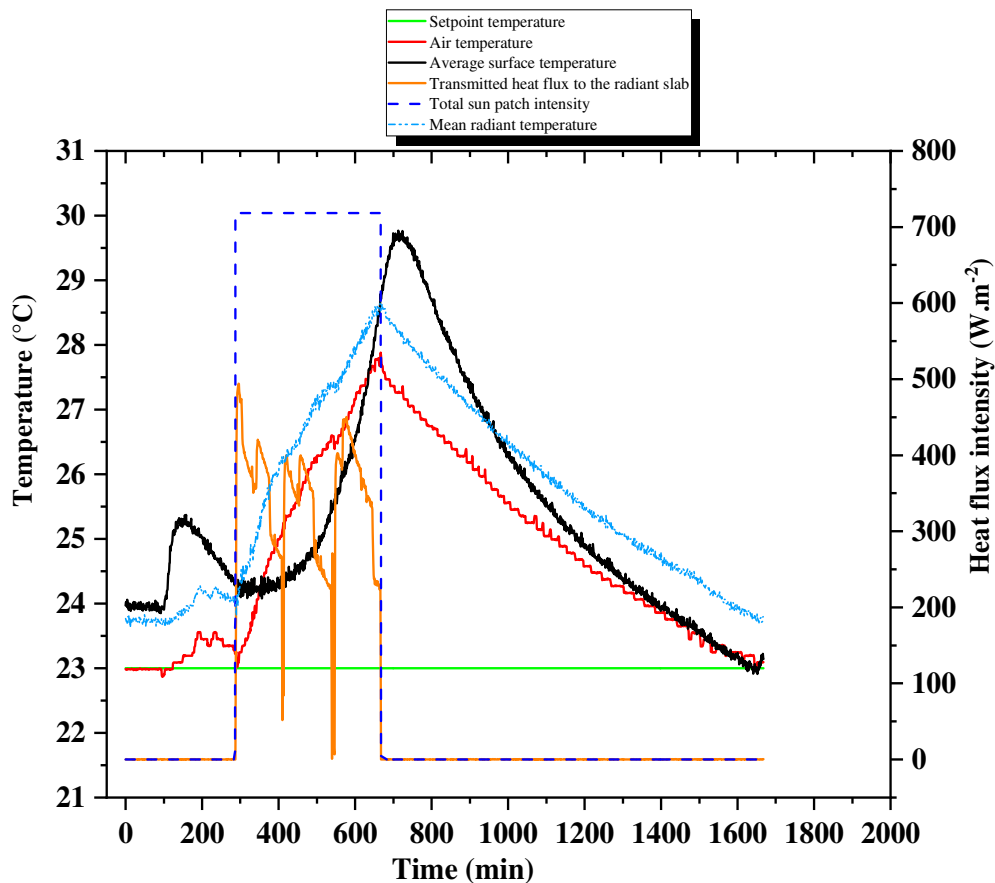
387 Despite changing the heating film position, the localized simulated sun patch acting for 2 h
 388 did not notably affect the thermal performance of the FHS. This is evident from the average
 389 slab surface temperature, which did not exceed the recommended upper limit of 28°C.
 390 Nevertheless, the inside zone air temperature reached 25°C, which is 2°C higher than the set
 391 point temperature, and was maintained at this temperature for approximately 700 min. The
 392 recommended upper limit of 24°C for human comfort was surpassed for approximately 300
 393 min. Moreover, the first and second tests showed that potential energy was saved due to the
 394 stored heat from the solar radiation, which can be utilized as a secondary heating source to
 395 minimize the overall daily FHS energy consumption. To make the best use of this energy, a
 396 more predictive control strategy for the FHS and the heating generator (i.e., heat pump) needs
 397 to be adopted during the mid-season when a sun patch radiation is expected.

398 4.3. Third scenario

399 Based on the results of the previous test scenarios, a third experimental test scenario was
 400 examined, in which a moving sun patch was reproduced on the heating floor slab surface for
 401 the duration of 6 h. As illustrated in Fig. 5c, the heating film was horizontally moved by 40
 402 cm from its initial location every 2 h, while the initial climatic conditions and the final air
 403 temperature set point of the inside zone were kept the same as in the previous tests.

404 As presented in Fig. 16 and 17, the sun patch was reproduced after the air temperature
405 reached 23°C. During this period, some minor fluctuations were observed in the surface
406 temperature along with a slight increase in air temperature, which is an expected response of
407 the FHS to stabilize the air temperature.

408



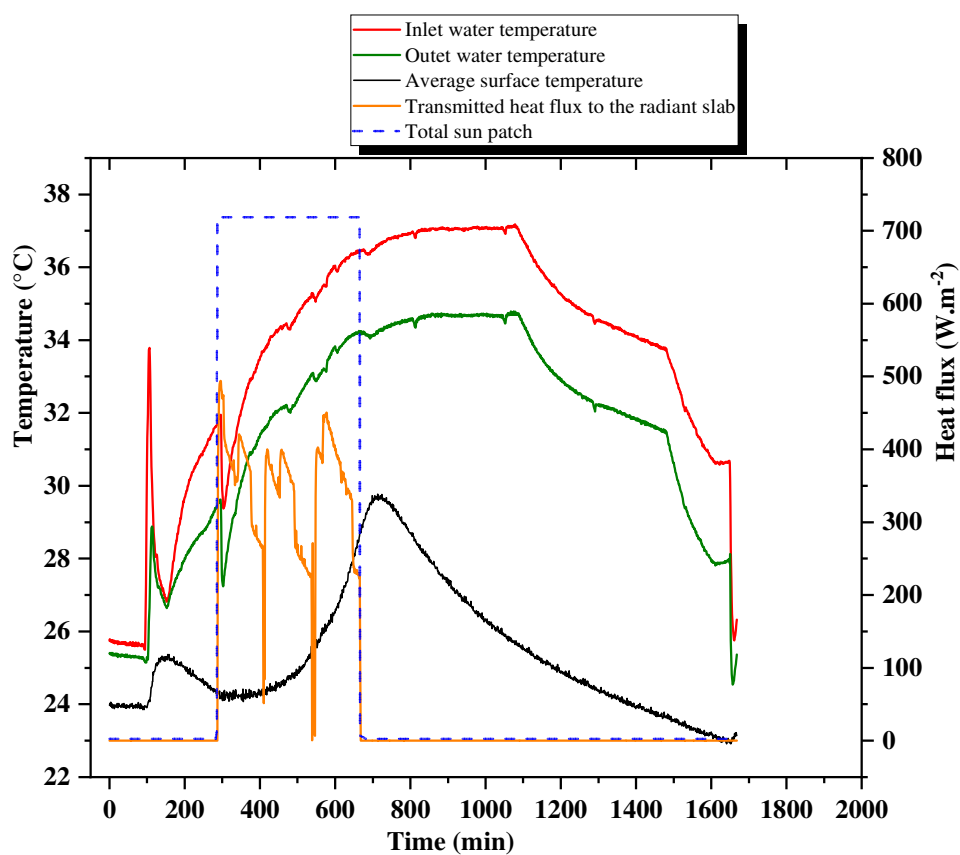
409

410 Figure 16: Average surface temperature, air temperature, and direct solar radiation intensity
411 profiles in the third test scenario.

412 When the heating film was turned-on, the air temperature increased instantaneously and
413 rapidly. During the 6 h of test to reproduce the artificial sun patch, the measured ambient air
414 temperature reached a maximum of 28°C, exceeding the recommended interior ambience
415 comfort temperature by 4°C. It is noteworthy that in the first minutes of sun patch application,
416 the average surface temperature of the heating floor remained almost constant and started to
417 increase only after approximately 176 min. In the third test scenario, we aimed at assessing
418 the dynamic thermal behavior of the radiant slab, which justifies the decision to place both the
419 surface temperature sensors away from the radiant film to obtain the measurements that

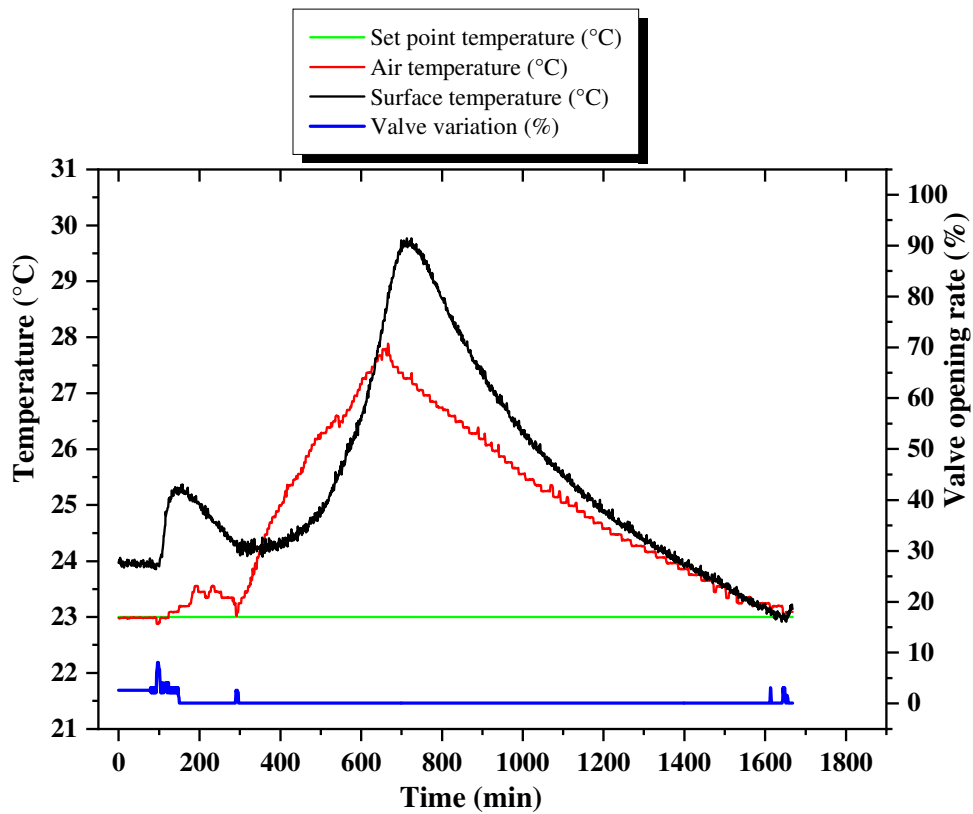
420 reflect the average floor surface temperature. Consequently, the heat transferred from the
421 radiant film will be first absorbed by the exposed part of the FHS and then spread over the
422 remaining part of the heating floor by the means of the embedded pipes and the horizontal
423 heat conduction over the slab surface. Moreover, the increase in air temperature will affect the
424 floor surface temperature.

425 Furthermore, although the thermostatic valve was fully closed (opening rate: 0%) during the
426 application of the sun patch (Fig. 18), the water continuously exchanged heat by conduction
427 inside the cross-linked pipes, which increased the average surface temperature to a peak value
428 of 30°C.



429

430 Figure 17: Inlet and outlet water temperature profiles in the third test scenario.



431

432 Figure 18: Thermostatic valve response during the third experiment.

433 Moreover, the effects of the simulated sun patch on the test cell are more remarkable for the
 434 air temperature variation. Hence, the overheating rates are:

435
$$\begin{cases} OR^s = 60.7 \% \\ OR^a = 12.1 \% \end{cases}$$

436 It is noteworthy that the effects of surface temperature elevation on the human body are less
 437 significant compared with the thermal discomfort caused by air temperature elevation. This
 438 corresponds to a significant potential energy saving of the FHS, which can be extremely
 439 useful from energy and economic perspectives. However, as mentioned above, a better
 440 regulation system is required for FHSs to achieve energy saving and avoid any overheating
 441 due to the solar patch, especially during mid-season.

442 The obtained results indicate two major overheating problems with the combined effects. The
 443 first is directly related to the presence of a sun patch on a FHS, which leads to an increase air
 444 temperature causing overheating, and the second is due to the floor thermal inertia that causes
 445 the heating process to continue for a long period after the solar patch disappears. The latter

446 causes the average floor surface temperature to exceed the standard value. Hence, it can be
447 stated that an important potential energy saving occurs whenever a solar patch appears on a
448 FHS.

449 **5. Conclusion, work limitations and perspectives**

450 In this work, an experimental study was conducted to quantify the effects of solar heat gains
451 on the dynamic thermal behavior of a radiant FHS and the indoor climatic conditions of a full-
452 scale test facility.

453 (i) Three major experimental scenarios were investigated, in which direct solar
454 radiation was applied on the surface of a FHS and experimentally simulated with a
455 radiant film. For the first and second scenarios, the aim was to reproduce direct
456 solar radiation in two different locations of the FHS with 2 h of sunshine. In these
457 tests, the thermal performance of the FHS was not considerably affected; however,
458 a slight overheating was observed due to an increase in air temperature and a
459 regulation problem of the examined system was identified. Additionally, as
460 observed from thermal infrared camera images, a surface-localized overheating
461 occurred due to the sun patch, which resulted in an increase in surface temperature
462 by 11–21 °C as compared with that of the non-exposed area.

463 (ii) Based on the results, we conducted a third test in which more pertinent results
464 were obtained concerning the FHS thermal behavior and the overall indoor
465 environment of the climatic chamber. An overheating problem was observed for
466 both the average surface temperature and ambient air temperature. The average
467 surface temperature reached a maximum of 30°C even after the radiant film was
468 shut off, resulting in increases in the overheating rates of the indoor air
469 temperature and surface temperature to 12.1% and 60.7%, respectively.

470 (iii) The fact that the solar intensity was kept constant (700 W.m^{-2}) and concentrated in
471 a specific area with a rectangular constant shape is a work limitation. Knowing
472 that the real sun patch depends on the geographic zone, makes the previous
473 parameters time-dependent, the related conclusions could be different from those
474 of this study. However, it is noticed that the considered heating film in the present
475 experimental study offers well-defined boundary conditions for further
476 comparisons with the results given by numerical models that one can develop for

477 the heating slab temperature dynamic behavior under the surface heating
478 solicitation.

479 (iv) The presented results highlight the necessity of an adaptive control strategy for
480 FHSs to enhance their efficiency and minimize energy consumption. The more
481 efficient approach will establish a smart control over FHSs that take advantage of
482 unexpected perturbations such as solar heat gains. Furthermore, a fundamental
483 future perspective of the present study will be the validation of the experimental
484 results through a numerical model, which will have a limitless ability to recreate
485 the effect caused by solar radiation for different locations on the floor, solar heat
486 flux intensity, and duration. The future numerical model will be a highly practical
487 tool for designers and building engineers aiming to efficiently use FHSs in a smart
488 and eco-friendly manner to minimize energy consumption and ensure and maintain
489 reliable thermal comfort conditions.

490 **Acknowledgements**

491 The authors gratefully acknowledge Grand-Est Region, Troyes Champagne Métropole,
492 European Regional Development Fund, and EPF Foundation for the financial support and
493 Météo France of Barberey-Saint-Sulpice for the technical support.

494 **Declarations of interest:** none

495 **References**

- 496 ASHRAE, 2016. 2016 ASHRAE Handbook—HVAC systems and equipment. American
497 Society of Heating, Refrigerating and Air conditioning Engineers Inc., Atlanta.
- 498 ANSI/ASHRAE. Standard 55, 2010. Thermal Environmental Conditions for Human
499 Occupancy, American Society of Heating, Refrigerating, and Air-Conditioning Engineers,
500 Atlanta.
- 501 Athienitis, A.K., 1997. Theoretical Investigation of thermal performance of a passive solar
502 building with floor radiant heating. *Sol. Energy* 61(5), 337–345.
- 503 Athienitis, A.K., Chen, Y., 2000. The effect of solar radiation on dynamic thermal
504 performance of floor heating systems. *Sol. Energy* 69 (3), 229–237.

505 Benzaama, M.H., Lachi, M., Maalouf, C., Mokhtari, A.M., Polidori, G., Makhlouf, M., 2016.
506 Study of the effect of sun patch on the transient thermal behaviour of a heating floor in
507 Algeria. *Energy Build.* 133, 257–270.

508 CSTB, 2006. Document Technique Unifié NF DTU 65.14 P1, Exécution des planchers
509 chauffants à eau chaude – Partie 1: Cahier des clauses techniques – Dalles désolidarisés
510 isolées. AFNOR. Centre Scientifique et technique du Batiment. (in French)

511 Candanedo, J.A., Amelie, A., Athienitis, A.K., 2011. Predictive control of radiant floor
512 heating and transmitted irradiance in a room with high solar gains. *ASHRAE Trans.* 117 (2),
513 652–665.

514 Holman, J.P., 2009. *Heat Transfer*, tenth ed. McGraw-Hill Higher Education, New York.

515 ISO 7730, 2005. *Ergonomics of the Thermal Environment-Analytical Determination and*
516 *Interpretation of Thermal Comfort Using Calculation of the PMV and PPD Indices and Local*
517 *Thermal Comfort Criteria*, International Organization for Standardization.

518 Joe, J., Karava, P., 2019. A model predictive control strategy to optimize the performance of
519 radiant floor heating and cooling systems in office buildings. *Applied Energy* 245, 65–77.

520 Karabay, H., Arici, M., Sandik, M., 2013. A numerical investigation of fluid flow and heat
521 transfer inside a room for floor heating and wall heating systems. *Energy Build.* 67, 471–478.

522 Kim, W.K., Olesen, B.W., 2015. Radiant heating and cooling systems: part 2. *ASHRAE J.* 57
523 (2), 28.

524 Li, Y.L., Han, M.Y., Liu, S.Y., Chen, G.Q., 2019. Energy consumption and greenhouse gas
525 emissions by buildings: A multi-scale perspective. *Build. Environ.* 151, 240–250.

526 Merabtine, A., Benelmir, R., El Ganaoui, M., 2013. Pseudo-bond graph model for the
527 analysis of the thermal behaviour of buildings. *Thermal Science* 17 (3), 723–732.

528 Privara, S., Siroky, J., Ferkl, L., Cigler, J., 2011. Model predictive control of a building
529 heating system: The first experience. *Energy Build.* 43 (2–3), 564–572.

530 Rhee, K.N., Kim, K.W., 2015. A 50 year review of basic and applied research in radiant
531 heating and cooling systems for the built environment. *Energy Build.* 91, 166–190.

- 532 Rodler, A., Virgone, J., Roux, J.-J., Hubert, J.L., 2014. Development and validation of a three
533 dimensional thermal transient numerical model with sun patch: Application to a low energy
534 cell. *Energy Build.* 87, 425–435.
- 535 Singh, M.C., Garg, S.N., 2010. An empirical model for angle-dependent g-values of glazings.
536 *Energy Build.* 42 (3), 375–379.
- 537 Tian, Z., Love, J.A., 2008. A field study of occupant thermal comfort and thermal
538 environments with radiant slab cooling. *Build. Environ.* 43 (10), 1658–1670.
- 539 Wang, D., Liu, Y., Wang, Y., Liu, J., 2014. Numerical and experimental analysis of floor heat
540 storage and release during an intermittent in-slab floor heating process. *Appl. Therm. Eng.* 62
541 (2), 398–406.
- 542 Weather Channel, InfoClimat [WWW Document]. < [https://www.infoclimat.fr/observations-](https://www.infoclimat.fr/observations-meteo/temps-reel/troyes-barbercy/07168.html)
543 [meteo/temps-reel/troyes-barbercy/07168.html](https://www.infoclimat.fr/observations-meteo/temps-reel/troyes-barbercy/07168.html) > (accessed 08.03.2019)
- 544 Zhao, K., Liu, X.H., Jiang, Y., 2013. Application of radiant floor cooling in a large open
545 space building with high-intensity solar radiation. *Energy Build.* 66, 246–257.
- 546 Zhao, K., Liu, X.H., Jiang, Y., 2014. On-site measured performance of a radiant floor
547 cooling/heating system in Xi'an Xianyang International Airport. *Sol. Energy* 108, 274–286.

Graphical abstract

